A Two-Stage Support Vector Machine and SqueezeNet System for Range-Angle and Range-Speed Estimation in a Cluttered Environment of Automotive MIMO Radar Systems

Zakaria Benyahia[1], *Mostafa* Hefnawi[2], *Mohamed* Aboulfatah[1], *Hassan* Abdelmounim[1], and *Taoufiq* Gadi[1]

[1] Hassan I University Settat, Morocco
[2] Royal Military College of Canada, Kingston, Ontario, Canada

Abstract. This paper proposes a two-stage deep-learning approach for frequency modulated continuous waveform multiple - input multiple - output (FMCW MIMO) radar embedded in cluttered and jammed environments. The first stage uses the support vector machine (SVM) as a feature extractor that discriminates targets from clutters and jammers. In the second stage, the angle, range, and Doppler estimations of the extracted targets are treated by the SqueezeNet deep convolutional neural network (DCNN) as a multilabel classification problem. The performance of the proposed hybrid SVM-SqueezeNet method is very close to the one achieved by the SqueezeNet only but with the advantage of identifying the type of targets and reducing the training time required by the SqueezeNet.

1 Introduction

Multi-input and multi-output (MIMO) radar systems have recently received considerable research interest in the automotive industry [1]-[7]. Unlike traditional phased-array radars in which a steered beam is used at the transmitter to scan a sector, MIMO radar systems transmit orthogonal waveforms from each omnidirectional antenna element simultaneously, allowing for a sector scan rate that is several times faster than steered beam radars [8]-[15]. The orthogonality of the waveforms can be achieved using multiplexing techniques such as time-division multiplexing (TDM), frequency division multiplexing (FDM), code division multiplexing (CDM), or space division multiplexing (SDM) [16]-[19]. Moreover, MIMO radar with collocated antennas can achieve a better spatial resolution and clutter interference rejection capability by combining all the transmitting paths in a virtual array with an extended aperture. MIMO radar signal processing techniques can be based on traditional techniques such as Fast Fourier Transform (FFT), Multiple Signal Classifier (MUSIC) [20], the Estimation of Signal Parameters via Rotational Invariance Techniques (ESPRIT) [21], and Minimum Variance Distortionless Response (MVDR) [22]. On the other hand, Deep neural networks (DNNs) have been proposed for MIMO radar systems as an alternative to traditional techniques that are computationally expensive and very sensitive to clutters and interferences [23]-[28]. In [23], a transfer learning-based deep convolutional neural network (DCNN) was proposed for distributed Frequency Modulated Continuous Wave (FMCW) MIMO radar systems. The DCNN was trained using 2D range-azimuth angle maps of stationary targets. Simulation results showed that the proposed DCNN gives high-resolution radar images compared to a single MIMO radar system. Their experiment was restricted to non-moving targets and did not consider any clutters or interferences. In [24], the focus was on targets classification only, which was achieved using the first stage of unsupervised pretraining followed by supervised fine-tuning of the convolutional layers to extract spatially localized features. In [25], a deep learning model was proposed to simultaneously estimate the range and direction of arrival of stationary targets. The system was built on existing architectures for DoA estimation and took into consideration the low-resolution ADCs constraints.

The You Only Look Once YOLO networks have also been actively applied to automotive radar in recent years [26]-[28]. In [26], the YOLO network was applied to the radar data in the range-angle domain to detect stationary targets and classify them with over 90% accuracy. The high angle resolution MUSIC was used to generate the range-angle images in a free clutter and interference environment.

In [27], the YOLO network detection and classification was based on the range-Doppler domain. In [28], the training of the YOLO network was based on the high-resolution radar sensor data to determine the type of detected object and estimate its moving direction as well.

Most of these methods were based on either the range-angle or the range-Doppler images that were generated using high-resolution techniques and did not consider clutters and interferences in their environment.

In this paper, we propose a deep learning network (DLN) to classify moving targets and estimate their range-angle-doppler in the presence of clutters and jammers. The proposed DL network is performed in two stages. In the first stage, radar cross-section (RCS)-based target classification is used with the support vector machine (SVM) to identify the type of targets and, at the same time, acts as a filter by extracting clutters and jammers. In the second stage, the range, angle, and Doppler estimations of the classified targets are treated by SqueezeNet as a multilabel classification problem. Since the clutters and jammers were rejected at the first stage, the SqueezeNet was trained in a free clutter and jammer environment, speeding up its training time. The training of the SqueezeNet was based on a low-resolution 2D FFT applied to the MIMO radar data cube.

2 SYSTEM MODEL

An FMCW MIMO radar with two transmitting (TX) antennas and four receiving (RX) antennas, as shown in Fig. 1, is considered. TDM waveforms are assumed where only one transmit antenna is activated at once. This system can be mounted on a vehicle to track the range, angle, and speed of the vehicles in front of it as shown in Fig. 2.

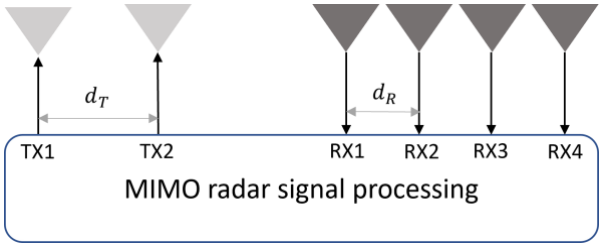

Fig. 1. Automotive radar(vehicle ego) and two target vehicles [29]

Fig. 2. MIMO radar with 2 transmitters and 4 receivers.

2.1 Virtual Array

When a MIMO radar transmits M independent orthogonal signals and receives echo returns with N receivers, a total of $M \times N$channels is processed, creating a virtual array of up to $M \times N$ receive elements. A received signal $\mathbf{x}(t)$ by the $MN-element$ receive virtual array can be expressed as [12]-[13]

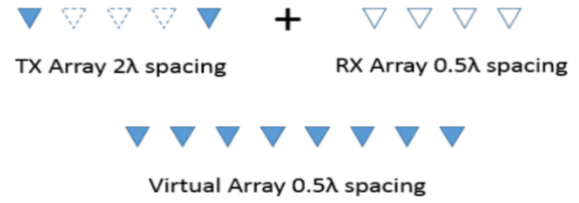

Fig. 3. Virtual array with 2 transmitters and 4 receivers [28]

$$\mathbf{x}(t) = \sum_{k=1}^{K} \boldsymbol{a}_k^v s_k(t) + \boldsymbol{n}(t) \quad (1)$$

where $\boldsymbol{a}_k^v = \boldsymbol{a}_k^T \otimes \boldsymbol{a}_k^R \in \mathbb{C}^{MN\times 1}$ is the steering vector of the virtual array due the k-th target, the Kronecker product is denoted by $\otimes$, the elements of $\boldsymbol{n}(t)$ are assumed to be independent and identically distributed complex Gaussian random vectors , $\boldsymbol{a}_k^T$ and $\boldsymbol{a}_k^R$ are the TX and RX steering vectors, respectively, and can be expressed as:

$$\boldsymbol{a}_k^T = \left(1, e^{j\left(\frac{2\pi}{\lambda}\right)d_T \sin\theta_k'}, \dots, e^{j(M-1)\left(\frac{2\pi}{\lambda}\right)d_T \sin\theta_k'}\right)^T \quad (2)$$

$$\boldsymbol{a}_k^R = \left(1, e^{j\left(\frac{2\pi}{\lambda}\right)d_R \sin\theta_k}, \dots, e^{j(N-1)\left(\frac{2\pi}{\lambda}\right)d_R \sin\theta_k}\right)^T \quad (3)$$

where d_T and d_R are the inter-element spacing of the TX and RX, respectively. θ_k' and θ_k are the direction of the k-th target with respect to transmit and receive arrays, respectively.

Using a virtual array allows the system to increase the resolution and accuracy beyond the physical number of elements present in the transmit and receive arrays. According to (1), the location of an element of the virtual can be expressed as follows

$$Virtaul\ Array(x) = \sum_{m=0}^{M-1}\sum_{n=0}^{N-1} \delta\big(x - (x_m + x_n)\big) \quad (4)$$

where x is the position across the array, x_m are the location of the transmit elements and x_n are the locations of the receive elements.

Fig. 3 shows the concept of the virtual array for the case of two TX elements and four RX elements. The aperture of the virtual array is dependent on the inter-element spacing of the TX and RX arrays. Therefore, to achieve the maximum angular resolution (i.e. 8-element virtual array) the interelement spacing of the TX array and the RX array are fixed at two wavelengths ($d_T = 2\lambda$) and half-wavelength ($d_R = \lambda/2$), respectively.

2.2 Radar Data Cube

The radar data cube is a convenient way to represent space-time processing conceptually. Fig. 4 shows the organization of the radar data cube. To extract the range and the velocity, the processor must perform an FFT along the fast-time axis and along the slow-time axis (for each pulse and each RF channel), respectively. To extract

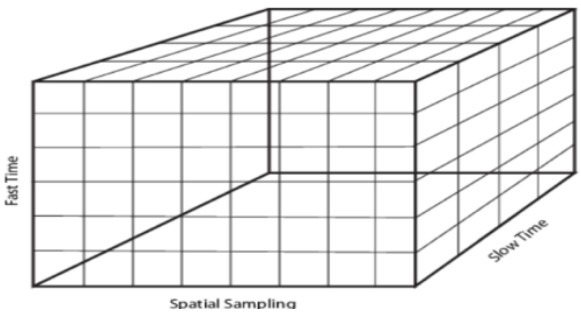

Fig. 4. Organization of Data Cube

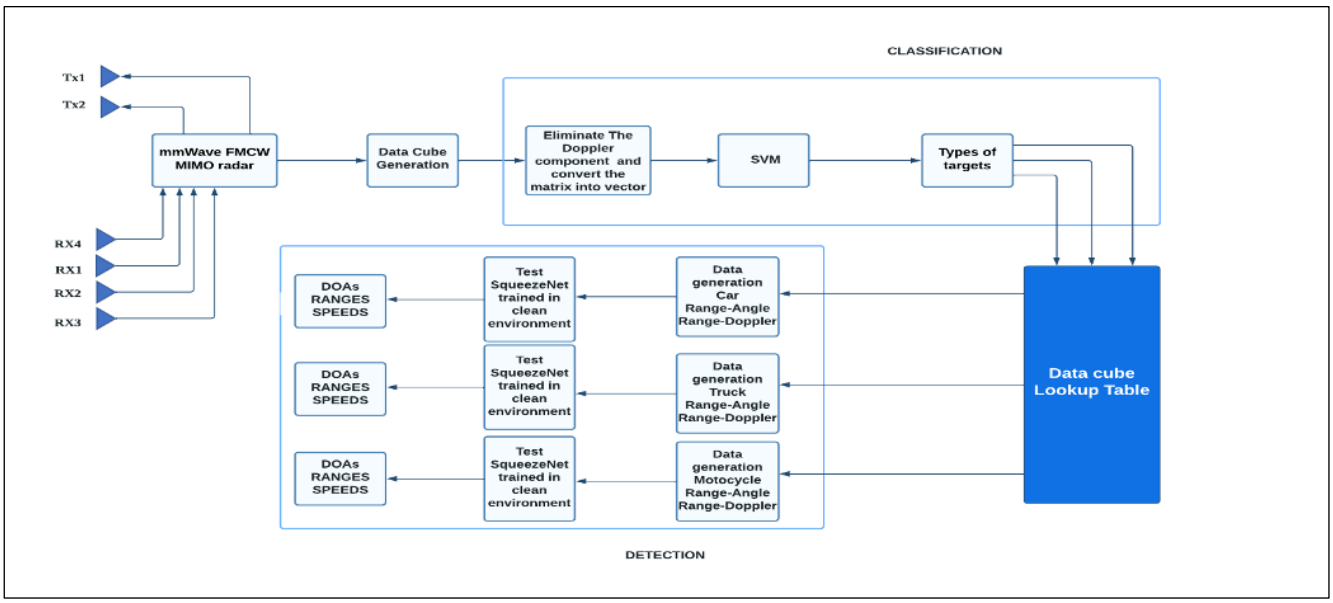

Fig. 5. Two-stage SVM-SqueezeNet Network for classification, Range-Angle Range-Doppler estimation, , and clutter/jammer rejection

the DOA, the processor must perform an FFT across the multiple array elements. For higher angular resolution, the FFT can be replaced with MUSIC, ESPRIT, or MVDR algorithms.

2.3 Proposed two-stage SVM-SqueezeNet Network

Fig. 5 shows the proposed two-stage SVM-SqueezeNet Network. The first stage uses the support vector machine (SVM) as a classifier. The SVM is a supervised learning algorithm used for classification and pattern learning problems. The objective of the SVM algorithm is to seek iteratively the hyperplanes that divide the datasets into classes and choose the optimal one that maximizes the margin between data points that belong to different classes and are closest to the hyperplane (Fig. 6). The data points that are closest to the hyperplane are called support vectors. SVM uses a set of mathematical functions called kernels that transforms input datasets into the desired form that makes them separable. Kernel functions can be of different types, summarized in Table I [29]. In this paper, the polynomial kernel function is used.

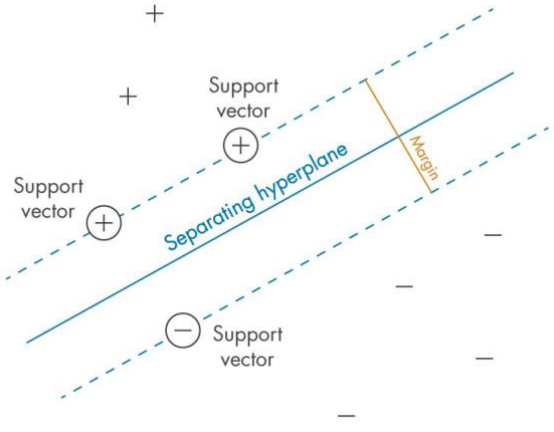

Fig. 6. Defining the "margin" between classes – the criterion that SVMs seek to optimize [29]

TABLE I. DIFFERENT TYPES OF KERNEL FUNCTIONS

Type of SVM	Mercer Kernel	Description
Gaussian or Radial Basis Function (RBF)	$K(x_1,x_2) = e^{(-\frac{\|x_1-x_2\|^2}{2\sigma^2})}$	One class learning. σ is the width of the kernel
Linear	$K(x_1,x_2) = x_1^T x_2$	Two class learning.
Polynomial	$K(x_1,x_2) = (x_1^T x_2 + 1)^p$	ρ is the order of the polynomial
Sigmoid	$K(x_1,x_2) = \tanh(\beta_0 x_1^T x_2 + \beta_1)$	It is a mercer kernel for certain β_0 and β_1 values only

The classification of the detected targets as trucks, cars, motorcycles or pedestrians was based on their RCSs, modelled according to [38] and summarized in Table II. Therefore, the Doppler dimension of the data cube was squeezed to provide a 2D matrix that is then entirely vectorized by concatenating the real and imaginary parts of each column. The size of the data cube used in this paper is $550 \times 8 \times 32$, and the specific converting process can be summarized as follows

$$Data\ cube^{(550\times8\times32)} \rightarrow A^{(550\times8)} = \begin{pmatrix} a_{11} & \cdots & a_{1\,8} \\ a_{21} & \cdots & a_{2\,8} \\ \vdots & \ddots & \vdots \\ a_{5501} & \cdots & a_{550\,8} \end{pmatrix}$$

$$\rightarrow B^{(4400\times1)} = \begin{pmatrix} a_{11} \\ \vdots \\ a_{550\,8} \end{pmatrix}$$

$$\rightarrow C^{(8800\times1)} = \begin{pmatrix} \Re e(B) \\ \Im m(B) \end{pmatrix}$$

TABLE II. RCS OF TARGETS

Category	RCS
Car	$\min(10\log10(R) + 5\ \text{dBsm}, 20\ \text{dBsm})$
Truck	$\min(10\log10(R) + 5\ \text{dBsm}, 45\ \text{dBsm})$
Motorcycle	7 dBsm
Pedestrian	-10 dBsm

The data set contains realizations of the following nine scenes:

- Two cars driving in a free clutter/jammer environment
- Two cars driving in a cluttered/jammed environment
- Two trucks driving in a free clutter/jammer environment
- Two trucks driving in a cluttered/jammed environment
- Two motorcyclists driving in a free clutter/jammer environment
- Two motorcyclists driving in a cluttered/jammed environment
- Two pedestrians walking in a free clutter/jammer environment
- Two pedestrians driving in a cluttered/jammed environment
- Clutters and jammers only

In each category, about 80% is reserved for the training data set while 20% is reserved for the test data set.

In the second stage, the SqueezeNet network predicts the range, angle, and Doppler of the already classified targets, namely "Car", "Motocycle," and "Truck". The SqueezeNet uses fire modules, as shown in Fig. 7 [30-31] to achieve high accuracy with smaller convolution neural network architecture.

Since the clutters and jammers are filtered out by the first stage, the SqueezeNet is trained in a clean environment, using pairs of DOAs, pairs of ranges and pairs of speeds for each type of target as shown in Table III, IV , and V.

The SqueezeNet requires data images for training and testing. Therefore, the range-angle and range-doppler images are generated by applying the 2D FFT to the MIMO radar data cube. Fig. 8 and Fig. 9 show the range-angle and range-speed plots, respectively, of two cars moving in a free clutter and interference environment with a pair of $azimuths = (2^o, 5^o)$, a pair of $ranges = (100\ \text{m}, 130\ \text{m})$ and a pair of $speeds = (36.111\ \text{m/s}, 41.66667\text{m/s})$. For the range-angle labelling, it is corresponding to the m^{th} pair of ranges and the n^{th} pair of angles, while it is referring to the m^{th} pair of ranges and the n^{th} pair of speeds for the range-speed labelling.

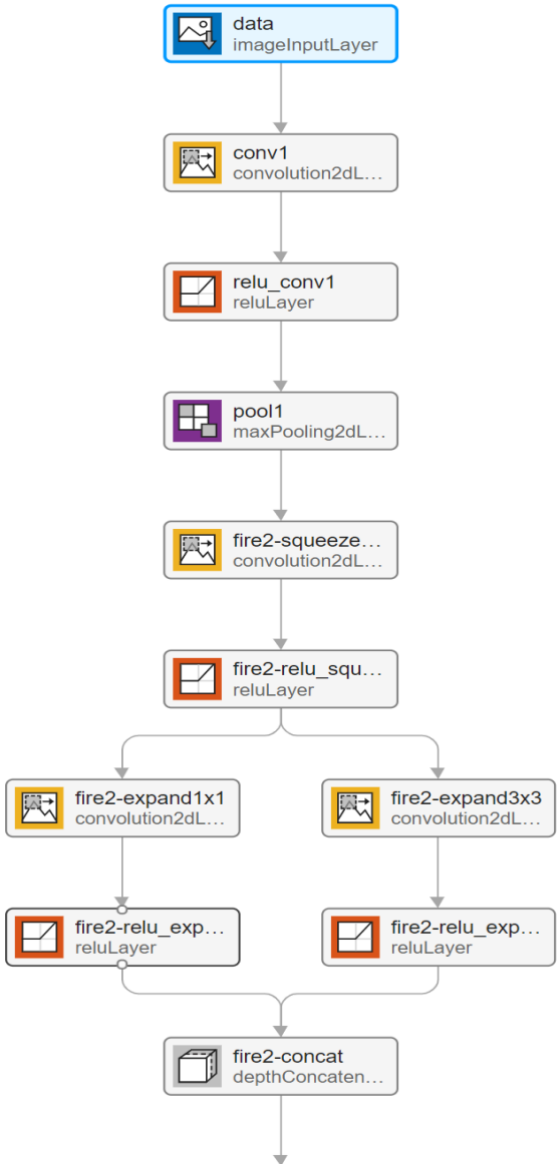

Fig. 7. SqueezeNet Fire Module [30]

The range-speed response of Fig. 9 shows that the targets are moving at the relative speeds of (–16.66 m/s, -22.22 m/s) with respect to the speed of the radar. It should be noted that the negative speeds indicate that the targets are moving away from the ego car.

Referring to Fig. 5, the data cube used for the training are indexed and placed in a lookup table. This indexation is used by the SVM predicted labels to allow tracing back the corresponding data cube. Table VI explains the indexation operation for the car predicted label case. The label "car" without clutter-jammer is found in indexes 1, 3 and 5. The first index 1 refers to the first pair of DOAs, the third index to the pair of ranges, and the sixth index to the pair of speeds. These indexes allow us to identify the data cube corresponding to these pairs, applied to the 2D FFT to generate the range-angle and range speed images. These images are then applied to the SqueezeNet to predict the ranges, DOAs, and speeds. The same process is applied to each type of target.

TABLE III. PAIRS OF RANGES, ANGLES, AND SPEEDS CAR

Pair	DOA (degrees)		RANGE (m)		SPEED (m/s)	
1	2	5	100	130	36.11	41.66
2	-1	5	70	130	30.55	41.66
3	-4	5	40	130	25	41.66
4	-7	5	70	100	19.44	41.66
5	-1	2	40	100	30.55	36.11
6	-4	2	40	70	25	36.11
7	-7	2			19.44	36.11
8	-4	-1			25	30.55
9	-7	-1			19.44	30.55
10	-7	-4			19.44	25

TABLE IV. PAIRS OF RANGES, ANGLES, AND SPEEDS MOTOCYCLE

Pair	DOA (degrees)		RANGE (m)		SPEED (m/s)	
1	6	9	80	100	22.22	27.77
2	3	9	60	100	16.66	27.77
3	0	9	40	100	11.11	27.77
4	3	6	20	100	5.55	27.77
5	0	6	60	80	16.66	22.22
6	0	3	40	80	11.11	22.22
7			20	80	5.55	22.22
8			40	60	11.11	16.66
9			20	60	5.55	16.66
10			20	40	5.55	11.11

TABLE V. PAIRS OF RANGES, ANGLES, AND SPEEDS TRUCK

Pair	DOA (degrees)		RANGE (m)		SPEED (m/s)	
1	3	6	110	140	33.33	38.88
2	0	6	80	140	27.77	38.88
3	-3	6	50	140	22.22	38.88
4	-6	6	80	110	16.66	38.88
5	0	3	50	110	27.77	33.33
6	-3	3	50	80	22.22	33.33
7	-6	3			16.66	33.33
8	-3	0			22.22	27.77
9	-6	0			16.66	27.77
10	-6	-3			16.66	22.22

TABLE VI. INDEXATION METHOD FOR THE LABEL CAR

Index	Predicted label	Angle	Range	Speed
1	Car	1	3	6
2	Truck	2	3	5
3	Car	1	3	4
4	Motorcycle	3	5	2
5	Car	7	2	1
6	Car with jammer	2	6	9

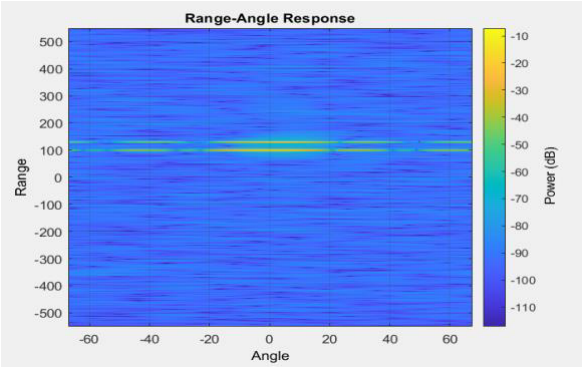

Fig. 8. Range-angle response of two cars moving in a free clutter/jammer environment.

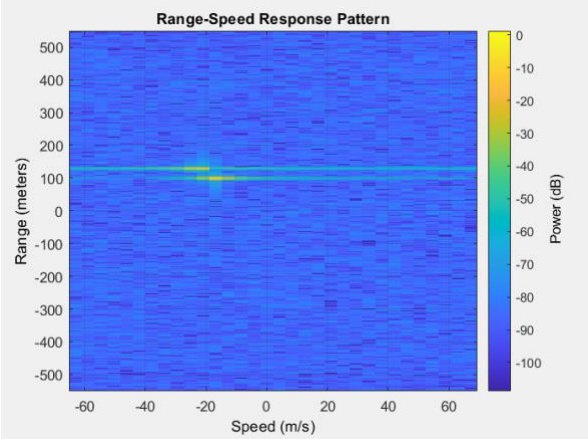

Fig. 9. Range-speed response of two cars moving in a free clutter/jammer environment.

3 EXPERIMENTS AND RESULTS

Table VII summarizes the data set and the labelling for the classification by the SVM. Eight labels are used for the training, and for each category, 80% is reserved for the training data set, while 20% is reserved for the test data set. The confusion matrix of Fig. 10 and Table VIII show the performance of the SVM. As it can be concluded, almost all of the eight types of targets are correctly identified by the network.

TABLE VII. SVM DATA SET AND THE LABELLING

Labels	Data Set	Training	Test
Car in a clean environment	600	480	120
Truck in a clean environment	600	480	120
Motocycle in clean environment	600	480	120
Car with Jammer and Clutter	3000	2400	600
Truck with Jammer and Clutter	3000	2400	600
Motocycle with Jammer and Clutter	3000	2400	600
Pedestrian	360	240	120
Pedestrian with Jammer and Clutter	1800	1200	600
Jammer and Clutter	21	16	5

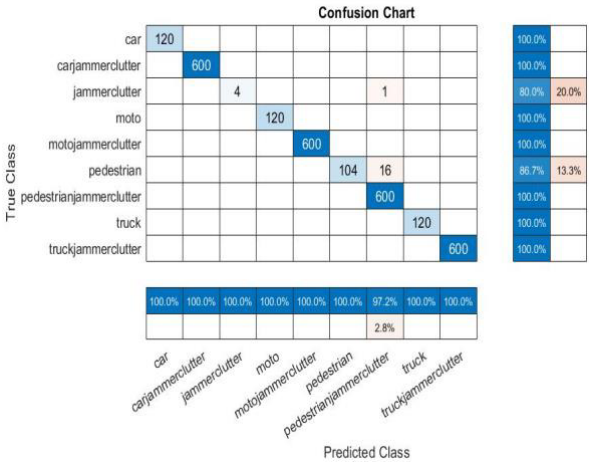

Fig. 10. Confusion chart for classification

TABLE VIII. PERFORMANCE OF SVM FOR CLASSIFICATION AND NOISE REJECTION

Architecture	SVM
No. of Classes	9
No. of Training Samples	10096
No. of Test Samples	2885
Validation Accuracy	99.6343%
Accuracy	99.4107%

On the other hand, Table IX shows the performance of the SqueezeNet, trained in a clean environment, for the range-angle and range-speed estimation of each type of target.

TABLE IX. PERFORMANCE OF SQUEEZENET IN A CLEAN ENVIRONMENT

Category		Car	Truck	Motocycle
Range-angle	Validation accuracy	100%	100%	100%
	Accuracy	98.33%	99%	99.1667%
Range-doppler	Validation accuracy	100%	100%	100%
	Accuracy	99%	99.23%	98.33%

The performance of the proposed hybrid SVM-SqueezeNet network is compared to the SqueezeNet only, which is trained in an environment with clutters and jammers. In this comparison, we focus on the detection aspect only, i.e. the range-angle and range-speed estimation of targets in the presence of clutters and jammers. According to Table III, the training is achieved with 60 labels. In the case of range-angle estimation, this corresponds to 6 pairs of ranges and 10 pairs of angles. Similarly, in the case of range-speed estimation, this corresponds to 6 pairs of speeds and 10 pairs of angles. For each type of target, there are 48 images (8 for clean environments, 32 for targets with jammer and 8 for targets with clutter).

Fig. 11 and Fig. 12 show the range-angle and range-doppler plots of two cars moving, in the presence of clutter and a jammer environment, with a pair of $azimuths = (2^o, 5^o)$, a pair of $ranges = (100\ \mathrm{m}, 130\ \mathrm{m})$ and a pair of $speeds = (36.11\ \mathrm{m/s}, 41.66\mathrm{m/s})$. The clutter signal was generated using the constant gamma model [39], with the gamma value set to -20 dB, typical for flatland clutter. For each range, the clutter return is a combination of the returns from many small clutter patches on that range ring, and each patch has an azimuth width of 10 degrees. On the other hand, the jammer signal was generated using the barrage jammer model, which is a strong, continuous white noise directed toward the radar receiver. It is assumed that the jammer is at a specific location, and the jamming signal is associated with a specific direction.

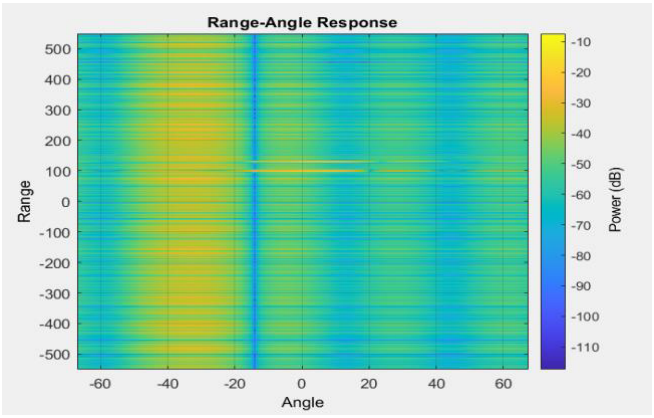

Fig. 11. Range-Angle response with clutter and jammer

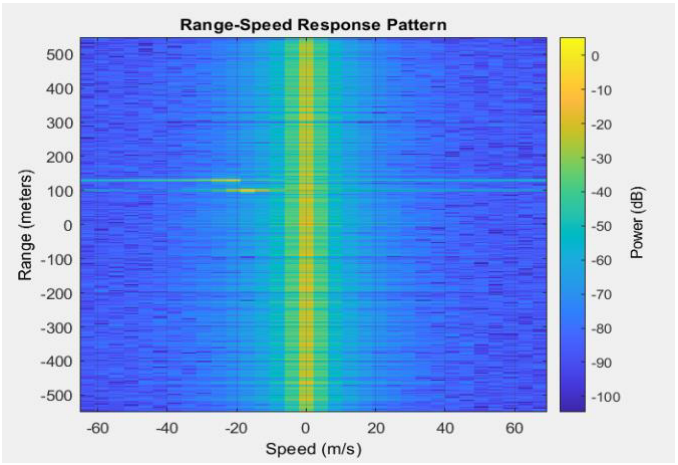

Fig. 12. Range-Speed response with clutter and jammer

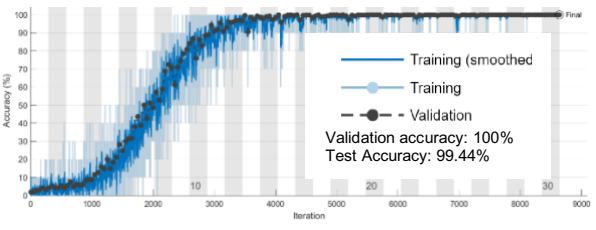

Fig. 13. Validation Accuracy of SqueezeNet Range-Speed

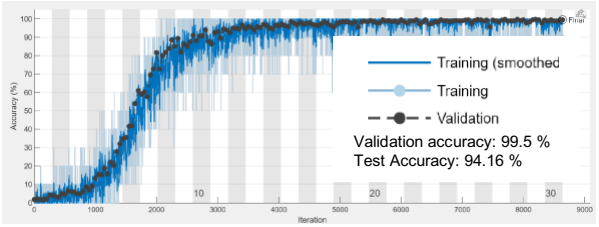

Fig. 14. Validation Accuracy of SqueezeNet Range-Angle

Fig. 13 and Fig. 14 show the validation accuracy of the SqueezeNet in the case of range-angle and range-speed estimation, respectively. The SqueezeNet model was trained with 2880 samples and tested with 720 samples for all 60 classes for 30 epochs. The training converges with a test accuracy of 94.16% for range-angle estimation and 99.44% for range-speed estimation. It is noted that in both cases, range-angle and range-speed estimation, the performance of the SqueezeNet is very close to the performance of the SqueezeNet trained in a clean environment but combined with the SVM.

4 Conclusion

A two-stage SVM-SqueezeNet approach was proposed for FMCW MIMO radar to classify and detect moving targets in a cluttered and jammed environment. The proposed approach reached an average accuracy of 98.33% in the range-angle estimation and 99 % in the case of range speed estimation. The performances are very close to the one achieved by the SqueezeNet only (94.44% for range-angle and 99.44% for range-speed) but with the advantage of identifying the type of targets and reducing the training time required by the SqueezeNet.

References

[1] O.Bialer , A.Jonas, and T.Tirer "Code Optimization for Fast Chirp FMCW Automotive MIMO Radar", IEEE Transactions on Vehicular Technology 70 (8), 7582-7593, July, 2021.

[2] M.Gottinger , M.Hoffmann, M. Christmann, M.Schutz, F. Kirsch, P.Gulden, and M.Vossiek Coherent Automotive Radar Networks: The Next Generation of Radar-Based Imaging and Mapping. IEEE Journal of Microwaves, vol. 1, no. 1, pp. 149 - 163, Januar, 2021.

[3] B.Li , S.Wang, Z.Feng , J.Zhang , X.Cao , and C.Zhao. Fast Pseudospectrum Estimation for Automotive Massive MIMO Radar. arXiv: 1911.07434v3, Dec 2021.

[4] M.Gottinger , M.Hoffmann, M. Christmann, M.Schutz, F. Kirsch, P.Gulden, and M.Vossiek Coherent Automotive Radar Networks: The Next Generation of Radar-Based Imaging and Mapping. IEEE Journal of Microwaves, vol. 1, no. 1, pp. 149 - 163, Januar, 2021.

[5] C.Pfeffer, R.Feger, C.Wagner and A.Stelzer. FMCW MIMO Radar System for Frequency-Division Multiple TX-Beamforming. IEEE transactions on microwavetheory and techniques vol. 61, no. 12, decembre 2013

[6] A.Bose , B.Tang , M.Soltanalian and J.Li. Mutual Interference Mitigation for Multiple Connected Automotive Radar Systems. IEEE Transactions on Vehicular Technology

[7] N.Amani , F.Jansen, A.Filippi , M .V.Ivashina, and Rob Maaskant. Sparse Automotive MIMO Radar for Super-Resolution Single Snapshot DOA Estimation With Mutual Coupling IEEE Access, vol. 9 ,2021

[8] P. Sévigny, "MIMO Radar: Literature survey of papers between 2003 and September 2008," DRDC, Ottawa, ON, TM 2008-333, Mar. 2009.

[9] J. Li and P. Stoica, MIMO Radar Signal Processing. Hoboken, NJ: Wiley-IEEE Press, 2008.

[10] P. W. Moo and Z. Ding, "Tracking Performance of MIMO Radar for Accelerating Targets," IEEE Trans. Signal Process., vol. 61, no. 21, pp. 5205–5216, Nov. 2013.

[11] I. Bekkerman and J. Tabrikian, "Target Detection and Localization Using MIMO Radars and Sonars," IEEE Trans. Signal Process., vol. 54, no. 10, pp. 3873–3883, Oct. 2006.

[12] E. Fishler, A. Haimovich, R. Blum, D. Chizhik, L. Cimini, and R. Valenzuela, ``MIMO radar: An idea whose time has come," in Proc. IEEE Radar Conf., Apr. 2004, pp. 71-78.

[13] F. C. Robey, S. Coutts, D. Weikle, J. C. McHarg, and K. Cuomo, ``MIMO radar theory and experimental results," in Proc. 28th Asilomar Conf. Signals, Syst. Comput., Nov. 2004, pp. 300-304.

[14] M. Hefnawi, J. Bray, J. Bathurst, and Y. Antar, "MIMO Radar Using a Vector Network Analyzer," Electronics, vol. 8, no. 12, Art. no. 12, Dec. 2019, doi: 10.3390/electronics8121447.

[15] J. Bergin and J. R. Guerci, MIMO Radar Theory and Application. Boston, MA, USA: Artech House, 2008.

[16] H. Sun, F. Brigui, and M. Lesturgie, "Analysis and comparison of MIMO radar waveforms," in 2014 International Radar Conference, 2014, pp. 1–6.

[17] Olivier Rabaste, Laurent Savy,Mathieu Cattenoz, and Jean-Paul Guyvarch. Signal waveforms and range/angle coupling in coherent colocated MIMO radar. In Radar (Radar), 2013 International Conference on, pages 157–162. IEEE, 2013.

[18] Ming Xue, Jian Li, and Peter Stoica. MIMO radar waveform design. In Fulvio Gini, Antonio DeMaio, and Lee Patton, editors,Waveformdesign and diversity for advanced radar systems, pages 89–120. IET Press, 2012.

[19] Hongbo Sun, Frédéric Brigui, and Marc Lesturgie. Analysis and comparison of MIMO radar waveforms. In 2014 International Radar Conference. IEEE, 2014.

[20] Ralpph O. Acmidt, "Multiple Emitter Location and Signal Parameter Estimation, "IEEE Trans. Antennas & Prop., vol. AP-34, no. 3, Mar. 1986, pp. 276-280

[21] R. Roy and T. Kailath, "ESPRIT-estimation of signal parameters via rotational invariance techniques," IEEE Trans. Acoust. Speech Signal Process., vol. 37, no. 7, pp. 984–995, Jul. 1989.

[22] J. Capon, "High-resolution frequency-wavenumber spectrum analysis," Proc. IEEE, vol. 57, no. 8, pp. 1408-1418, Aug. 1969.

[23] Jiho Seo , Yunji Yang , Yong‐gi Hong , Jaehyun Park, "Transfer learning‐based radar imaging with deep convolutional neural networks for distributed frequency modulated continuous waveform multiple‐input multiple‐output radars," IET Radar, Sonar & Navigation, 2021;15:1209–1220; doi: 10.1049/rsn2.12105.

[24] M. S. Seyfioglu, A. M. Ozbayoglu, and S. Z. Gurbuz, "Deep convolutional autoencoder for radar-based classification of similar aided and unaided human activities," IEEE Transaction on Aerospace and Electronic Systems. Vol. 54, no. 4 Aug. 2018.

[25] Ramakrishna Sai Annaluru , Khurram Usman Mazher, Robert W. Heath, "Deep Learning Based Range and Doa Estimation using low Resolution FMCW Radars," 2021 IEEE Statistical Signal Processing Workshop (SSP), DOI: 10.1109/SSP49050.2021.9513759.

[26] Woosuk Kim 1, Hyunwoong Cho , Jongseok Kim, Byungkwan Kim, and Seongwook Lee , "YOLO-Based Simultaneous Target Detection and Classification in Automotive FMCW Radar Systems," Sensors 2020, 20(10), 2897.

[27] Pérez, R.; Schubert, F.; Rasshofer, R.; Biebl, E. Deep learning radar object detection and classification for urban automotive scenarios. In Proceedings of the 2019 Kleinheubach Conference, Miltenberg, Germany, 23–25 September 2019.

[28] Jin-Cheol Kim, Hwi-Gu Jeong, and Seongwook Lee," Simultaneous Target Classification and Moving Direction Estimation in Millimeter-Wave Radar System," Sensors 2021, 21(15), 5228.

[29] Support Vector Machine (SVM) MATLAB, [Online]. Available:https://www.mathworks.com/discovery/support-vector-machine.html?s_tid=srchtitle_Support%20Vector%20Machine_1

[30] F. N. Iandola, S. Han, M. W. Moskewicz, K. Ashraf, W. J. Dally, and K. Keutzer. SqueezeNet: AlexNet-level accuracy with 50x fewer parameters and< 0.5 MB model size. arXiv preprint arXiv:1602.07360, 2016.

[31] SqueezeNet,[Online]. Available:https://www.mathworks.com/help/deeplearning/ref/squeezenet.html

[32] Radar Target Classification Using Machine Learning and Deep Learning-MATLAB,[Online]. Available:https://www.mathworks.com/help/radar/ug/radar-target-classification-using-machine-learning-and-deep-learning.html

[33] T.Cheng , B.Wang , Z.Wang , R.Dong , and B.Cai. Lightweight CNNs-Based Interleaved Sparse Array Design of Phased-MIMO Radar, IEEE sensors journal, vol. 21, no. 12, june 15, 2021

[34] T.Wan , X.Fu , K.Jiang , Y.Zhao and B.Tang. Radar Antenna Scan Pattern Intelligent Recognition Using Visibility Graph, IEEE access, volume 7, 2019

[35] F.Meng , K.Tian, and C.Wu Deep Reinforcement Learning-Based Radar Network Target Assignment, Electronics, vol. 11, no. 3, January 2022, doi: 10.3390/electronics11030311

[36] Increasing Angular Resolution with Virtual Arrays-MATLAB, [Online]. Available:https://www.mathworks.com/help/phased/ug/increasing-angular-resolution-with-mimo-radars.html.

[37] Automotive Adaptive Cruise Control Using FMCW Technology [Online].Available:https://www.mathworks.com/help/radar/ug/automotive-adaptive-cruise-control-using-fmcw-technology.html.

[38] Karnfelt, Camilla, et al. "77 GHz ACC Radar Simulation Platform." 9th International Conference on Intelligent Transport Systems Telecommunications, (ITST), IEEE, 2009 , pp. 209–14.

[39] Barton, David. "Land Clutter Models for Radar Design and Analysis," Proceedings of the IEEE. Vol. 73, Number 2, February, 1985, pp. 198–204